

E14-2010-26

D. P. Kozlenko¹, N. T. Dang^{1,2}, Z. Jiráček³, S. E. Kichanov¹,
E. V. Lukin¹, B. N. Savenko¹, L. S. Dubrovinsky⁴, C. Lathe⁵

STRUCTURAL AND MAGNETIC PHASE TRANSITIONS
IN $\text{Pr}_{0.15}\text{Sr}_{0.85}\text{MnO}_3$ AT HIGH PRESSURE

¹Joint Institute for Nuclear Research, Dubna

²Tula State University, 300600 Tula, Russia

³Faculty of Nuclear Science and Physics Engineering, Břehová 7, 115 19
Prague 1, Czech Republic

⁴Bayerisches Geoinstitut, University of Bayreuth, D-95440 Bayreuth, Ger-
many

⁵Helmholtz Centre Potsdam, Telegrafenberg, 14407 Potsdam, Germany

Козленко Д. П. и др.

E14-2010-26

Структурные и магнитные фазовые переходы в $\text{Pr}_{0,15}\text{Sr}_{0,85}\text{MnO}_3$ при высоком давлении

Кристаллическая и магнитная структура манганита $\text{Pr}_{0,15}\text{Sr}_{0,85}\text{MnO}_3$ была исследована методами рентгеновской и нейтронной дифракции в температурном диапазоне 10–400 К при высоких внешних давлениях до 55 и 4 ГПа соответственно. При высоком давлении обнаружен структурный фазовый переход из кубической в тетрагональную фазу с положительным барическим коэффициентом для критической температуры перехода — $dT_{\text{ct}}/dP = 26(2)$ К/ГПа. Ниже $T_{\text{N}} \approx 280$ К формируется антиферромагнитное (АФМ) состояние С-типа. При нормальных условиях температуры структурного и магнитного фазовых переходов совпадают: $T_{\text{ct}} \approx T_{\text{N}}$. При высоком давлении они становятся различными: $T_{\text{N}} \ll T_{\text{ct}}$ — из-за более слабой барической зависимости T_{N} с коэффициентом $dT_{\text{N}}/dP = 3,8(1)$ К/ГПа.

Работа выполнена в Лаборатории нейтронной физики им. И. М. Франка ОИЯИ.

Сообщение Объединенного института ядерных исследований. Дубна, 2010

Kozlenko D. P. et al.

E14-2010-26

Structural and Magnetic Phase Transitions in $\text{Pr}_{0,15}\text{Sr}_{0,85}\text{MnO}_3$ at High Pressure

The crystal and magnetic structures of $\text{Pr}_{0,15}\text{Sr}_{0,85}\text{MnO}_3$ manganite have been studied by means of powder X-ray and neutron diffraction in the temperature range 10–400 K at high external pressures up to 55 and 4 GPa, respectively. A structural phase transition from cubic to tetragonal phase upon compression was observed, with large positive pressure coefficient of transition temperature $dT_{\text{ct}}/dP = 26(2)$ K/GPa. The C-type antiferromagnetic (AFM) ground state is formed below $T_{\text{N}} \approx 280$ K. While at ambient pressure the structural and magnetic transition temperatures coincide, $T_{\text{ct}} \approx T_{\text{N}}$, upon compression they become decoupled with $T_{\text{N}} \ll T_{\text{ct}}$ due to much weaker T_{N} -pressure dependence with coefficient $dT_{\text{N}}/dP = 3.8(1)$ K/GPa.

The investigation has been performed at the Frank Laboratory of Neutron Physics, JINR.

Communication of the Joint Institute for Nuclear Research. Dubna, 2010

INTRODUCTION

Manganites of perovskite type $\text{Ln}_{1-x}\text{A}_x\text{MnO}_3$ (Ln — lanthanum or rare earth, A — alkali earth elements) exhibit rich magnetic and electronic phase diagrams depending on the kind of Ln, A elements and their ratio [1]. These systems show for particular compositions an extreme sensitivity of magnetic, structural, electronic, transport properties to external fields, and have attracted considerable interest with respect to the recently discovered colossal magnetoresistance (CMR) effect.

The properties of manganites depend substantially on a balance between the ferromagnetic (FM) interactions mediated by itinerant charge carriers (double-exchange mechanism [2–4]) and the superexchange interactions between localized spins of manganese ions, which are usually antiferromagnetic (AFM) [5]. The FM double exchange is usually stronger than AFM superexchange for the doping levels $x < 0.5$, while for higher x values AFM superexchange interaction becomes dominant. Thus, magnetic phase diagrams of manganites with a large average radius of A-site cation $\langle r_A \rangle$ — $\text{La}_{1-x}\text{Sr}_x\text{MnO}_3$ [6], $\text{Pr}_{1-x}\text{Sr}_x\text{MnO}_3$ [6, 7] and to some extent also $\text{Nd}_{1-x}\text{Sr}_x\text{MnO}_3$ [8] follow in narrow composition range $0.45 < x < 0.85$ a general trend in the evolution of magnetic ground states: FM metallic \rightarrow A-type AFM metallic \rightarrow C-type AFM insulating state.

Recently it was found that the application of high pressure also leads to modifications of magnetic structure of $\text{Pr}_{1-x}\text{Sr}_x\text{MnO}_3$ manganites, $x \sim 0.5$ [9, 10]. In $\text{Pr}_{0.52}\text{Sr}_{0.48}\text{MnO}_3$ a suppression of the initial FM state and appearance of the A-type AFM ground state were observed. In $\text{Pr}_{0.44}\text{Sr}_{0.56}\text{MnO}_3$ with the initial A-type AFM ground state at ambient pressure an onset of the C-type AFM state was revealed at high pressure [9]. These high-pressure effects were successfully explained on the basis of the theoretical calculations of the generalized phase diagram of manganites with a doping level $x > 0.5$ [11] in terms of enhancement of the superexchange AFM interactions upon the bond lengths contraction.

While previous studies of $\text{Pr}_{1-x}\text{Sr}_x\text{MnO}_3$ were mainly focused on $x \sim 0.5$ region, high-pressure behavior of compounds with larger x values in the vicinity of the boundary between C-type and G-type AFM states of the magnetic phase diagram still remains unclear. In the present study, we have investigated the crystal and magnetic structure of $\text{Pr}_{0.15}\text{Sr}_{0.85}\text{MnO}_3$ manganite by X-ray and neutron diffraction at high pressures up to 55 and 4 GPa, respectively.

1. EXPERIMENTAL

The $\text{Pr}_{0.15}\text{Sr}_{0.85}\text{MnO}_3$ compounds were prepared by solid-state reaction at high temperature. Homogenized mixtures of Pr_6O_{11} , SrCO_3 and MnO_2 were first heated three times at $1000\text{ }^\circ\text{C}$ with intermediate grindings to achieve decarbonation. The powders were then pressed into pellets and sintered at $1500\text{ }^\circ\text{C}$ in air for 12 h. Afterwards, the sintered samples were slowly cooled to room temperature.

The angle-dispersive X-ray diffraction patterns at high pressures up to 55 GPa and ambient temperature were measured at the system consisting of a high-brilliance FRD rotating anode generator (Mo K_α radiation with $\lambda = 0.7115\text{ \AA}$) FluxMax focusing optics, and Bruker APEX CCD area detector [12]. The two-dimensional XRD images were converted to convention alone-dimensional diffraction patterns using the FIT2D program [13]. The sample was loaded in diamond anvils cell [12] in the Re gasket with admixed LiF as a pressure transmitting medium. The pressure was determined by the ruby fluorescence technique.

Additional energy-dispersive X-ray diffraction experiments at pressures up to 4 GPa in the temperature range 290–400 K were carried out at the beamline F2.1 (HASYLAB–DESY, Hamburg) using the multianvil X-ray system MAX80. The sample was placed in the cylindrical boron nitride container with an internal diameter of 1 mm. The upper half was filled with the sample, the lower half contained sodium chloride powder for pressure calibration. The cubic boron-epoxy chamber with sample container was compressed by six tungsten carbide anvils in a large hydraulic press. Diffraction spectra were recorded in an energy-dispersive mode using white synchrotron X-rays from the storage ring DORIS III. The ring operated at 4.5 GeV and a positron current of 80–150 mA. The incident X-ray beam was collimated to $100 \times 100\text{ }\mu\text{m}$ with a divergence smaller than 0.3 mrad. Spectra were recorded by a Ge solid-state detector with a resolution of 153 eV at 5.9 keV resulting in a resolution of diffraction patterns of $\Delta d/d \approx 1\%$. The Bragg angle 2θ was fixed at 9.089° , counting times for each diffraction pattern were about 10 min.

Neutron powder diffraction measurements at high external pressures up to 4 GPa were performed at selected temperatures in the range 16–300 K with the DN-12 spectrometer [14] at the IBR-2 high-flux pulsed reactor (FLNP JINR, Dubna, Russia) using the sapphire anvil high-pressure cells [15]. The sample volume was about 2 mm^3 . A special cryostat constructed on the base of closed cycle helium refrigerator was used to create a low temperature on the sample. Several tiny ruby chips were placed at different points of the sample surface. The pressure was determined by the ruby fluorescence technique with the accuracy of 0.05 GPa at each ruby chip and the pressure value on the sample was determined by averaging of values obtained at different points. The estimated inhomogeneity of the pressure distribution on the sample surface was less than 15%. Diffraction

patterns were collected at scattering angles 45.5 and 90°. The spectrometer resolution at $\lambda = 2 \text{ \AA}$ is $\Delta d/d = 0.022$ and 0.015 for these angles, respectively. The typical data collection time at one temperature was 20 h.

Experimental data were analyzed by the Rietveld method using MRIA [16] and Fullprof [17] programs.

2. RESULTS AND DISCUSSION

2.1. X-Ray Diffraction. The X-ray diffraction patterns of $\text{Pr}_{0.15}\text{Sr}_{0.85}\text{MnO}_3$ at selected pressures and ambient temperature are shown in Fig. 1.

At ambient conditions, the cubic phase with space group $Pm\bar{3}m$ was evidenced. At pressures above 2 GPa a splitting of diffraction peaks at $2\theta = 21.2^\circ$ was observed, indicating a structural transition to a phase with lower symmetry. From the analysis of experimental data by the Rietveld method it was found

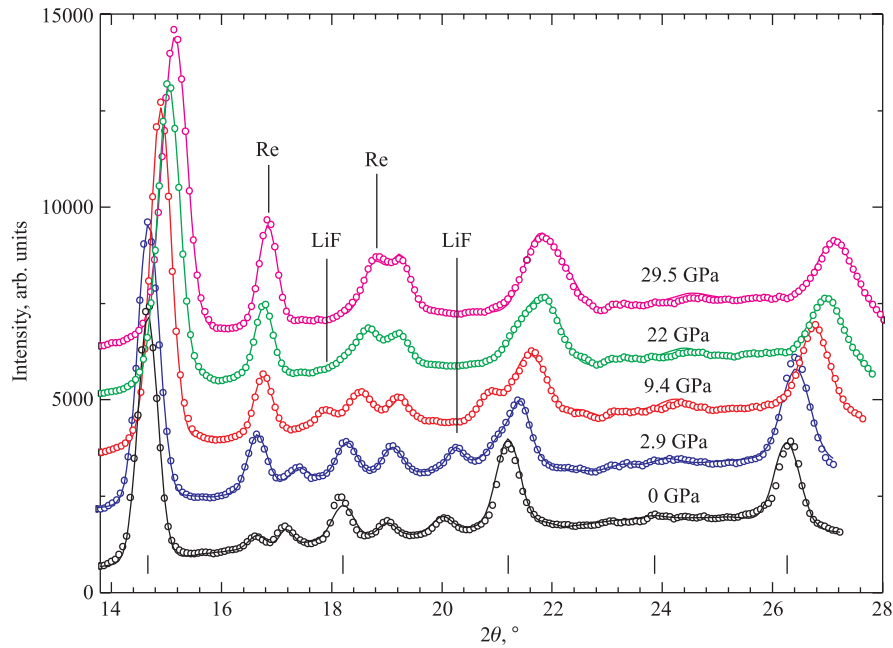


Fig. 1. X-ray diffraction patterns of $\text{Pr}_{0.15}\text{Sr}_{0.85}\text{MnO}_3$ measured at pressures $P = 0, 2.9, 9.4, 22.0, 29.5$ GPa at room temperature and processed by the profile matching method. The experimental points, calculated profile and Bragg peak positions for cubic phase (at $P = 0$ GPa) are shown. The addition diffraction peaks from high-pressure cell materials are marked

that high-pressure phase of $\text{Pr}_{0.15}\text{Sr}_{0.85}\text{MnO}_3$ has the tetragonal $I4/mcm$ symmetry. The unit cell of this structure is quadrupled with respect to the simple perovskite subcell (lattice parameters $a_t \approx a_p\sqrt{2}$ and $c_t \approx 2a_p$). The cubic to tetragonal transition occurs in $\text{Pr}_{0.15}\text{Sr}_{0.85}\text{MnO}_3$ at ambient pressure on cooling at $T_{\text{ct}} \approx 280$ K and observation of tetragonal phase at high pressures and ambient temperature implies a positive value of dT_{ct}/dP pressure coefficient.

The pressure dependences of lattice parameters and unit-cell volume for tetragonal phase of $\text{Pr}_{0.15}\text{Sr}_{0.85}\text{MnO}_3$ were shown in Fig. 2. The volume compressibility data were fitted by the third-order Birch–Murnaghan equation of state [18]:

$$P = \frac{3}{2}B_0 \left(x^{-7/3} - x^{-5/3} \right) \left[1 + \frac{3}{4}(B' - 4) \left(x^{-2/3} - 1 \right) \right], \quad (1)$$

where $x = V/V_0$ is the relative volume change, V_0 is the unit-cell volume at $P = 0$; B_0 and B' are the bulk modulus $B_0 = -V(dP/dV)_T$ and its pressure derivative $B' = (dB_0/dP)_T$. The calculated values for tetragonal phase of $\text{Pr}_{0.15}\text{Sr}_{0.85}\text{MnO}_3$ are $B_0 = 225(8)$ GPa, $B' = 4(1)$ and $V_0 = 223.4(8)$ Å³ are comparable with those found for $\text{Pr}_{0.52}\text{Sr}_{0.48}\text{MnO}_3$ [10] and $\text{La}_{0.5}\text{Ca}_{0.5}\text{MnO}_3$ [19].

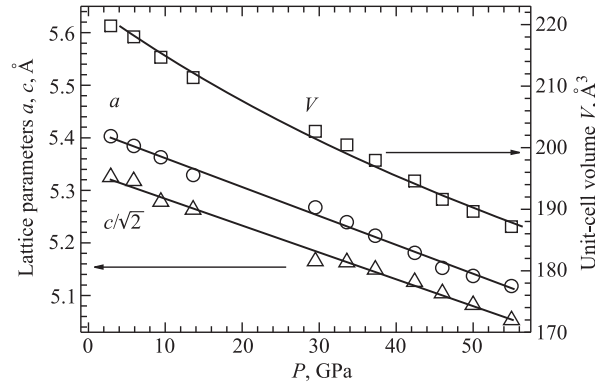


Fig. 2. Pressure dependences of the unit-cell volume fitted by the Birch–Murnaghan equation of state and lattice parameters of $\text{Pr}_{0.15}\text{Sr}_{0.85}\text{MnO}_3$ at room temperature fitted by linear functions

In order to study pressure evolution of the cubic–tetragonal transition temperature, additional energy-dispersive X-ray diffraction experiments were performed at pressures up to 4 GPa. The structural phase transition point was clearly indicated by appearance of splitting between (220) and (004) diffraction peaks (Fig. 3).

The obtained pressure dependence of T_{ct} demonstrates a linear increase with rather large coefficient $dT_{\text{ct}}/dP = 26(2)$ K/GPa. The thermal expansion coefficients $\alpha = 1/V (dV/dT)_p$ for $\text{Pr}_{0.15}\text{Sr}_{0.85}\text{MnO}_3$ were calculated to

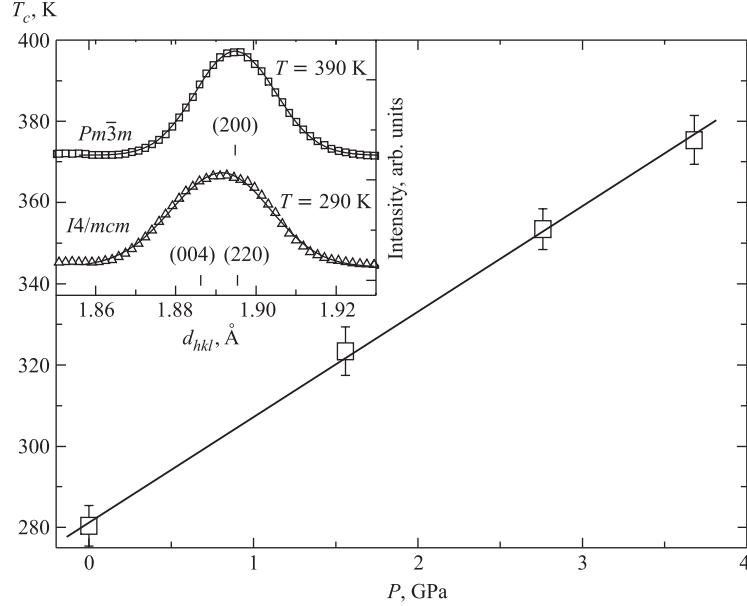


Fig. 3. The pressure dependence of cubic–tetragonal phase transition temperature. Solid lines represent linear fits to the experimental data. In insert: The parts of X-ray diffraction spectra at pressure $P = 1.6$ GPa and at ambient temperature and $T = 390$ K

be $1.23(8) \cdot 10^{-5} \text{ K}^{-1}$ for cubic phase and $1.4(5) \cdot 10^{-5} \text{ K}^{-1}$ for tetragonal phase at $P = 3.7$ GPa.

2.2. Neutron Diffraction. Neutron diffraction patterns of $\text{Pr}_{0.15}\text{Sr}_{0.85}\text{MnO}_3$ taken at $P = 0$ and 2.2 GPa, $T = 300$ and 16 K are shown in Fig. 4. On cooling, appearance of magnetic peaks located at $d_{hkl} \approx 3.15$ and 5.32 Å was observed below Neel temperature, $T_N = 280$ K at $P = 0$ (Fig. 4), evidencing the formation of the C-type AFM state [7, 20]. At ambient pressure, the onset of long-range magnetic order is accompanied by the structural transformation from cubic to tetragonal phase, while at $P > 2.2$ GPa it occurs within the tetragonal phase of $I4/mcm$ symmetry.

In the C-type AFM structure manganese moments form ferromagnetic chains along the tetragonal c -axis with antiferromagnetic coupling between neighboring chains [7, 20]. The analysis of temperature dependences of Mn magnetic moments shows that T_N value increases upon compression with pressure coefficient $dT_N/dP = 3.8(9) \text{ K/GPa}$ (Fig. 5), which is much smaller than that for cubic–tetragonal structural phase transition, $dT_{ct}/dP = 26(2) \text{ K/GPa}$.

The calculated from the Rietveld refinement of neutron diffraction data structural parameters for the cubic and tetragonal phases of $\text{Pr}_{0.15}\text{Sr}_{0.85}\text{MnO}_3$ at se-

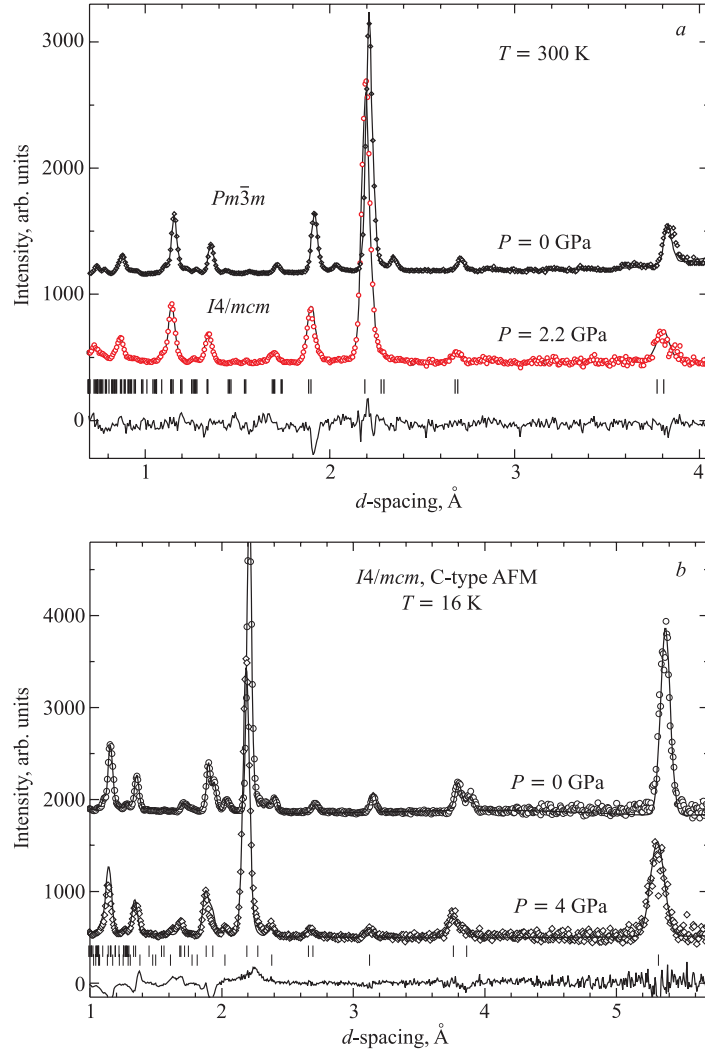


Fig. 4. Neutron diffraction patterns of $\text{Pr}_{0.15}\text{Sr}_{0.85}\text{MnO}_3$ measured at $P = 0$ and 2.2 GPa, $T = 300$ (a) and 16 K (b) at scattering angle $2\theta = 90^\circ$ and processed by the Rietveld method. The experimental points, calculated profile and difference curve (for $P = 4$ GPa) are shown. Ticks represent the calculated positions of the nuclear peaks of the $I4/mcm$ tetragonal phase and magnetic peaks of the C-type AFM state

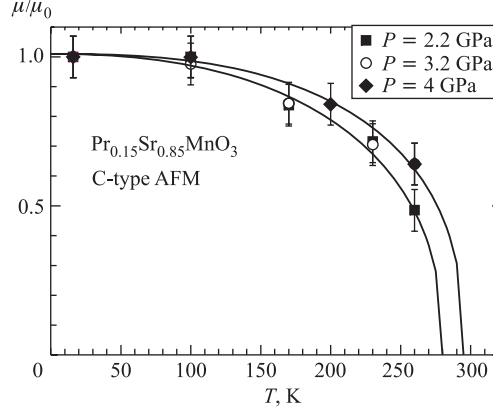


Fig. 5. Temperature dependences of Mn magnetic moments for the C-type AFM tetragonal phase of $\text{Pr}_{0.15}\text{Sr}_{0.85}\text{MnO}_3$ normalized to the moment value for $T = 16$ K at different pressures. The line is a guide for eye only

Structural parameters of $\text{Pr}_{0.15}\text{Sr}_{0.85}\text{MnO}_3$ manganites at different pressures and temperatures. In the cubic phase (space group $Pm\bar{3}m$) atomic positions are: Pr/Sr — 1(a) (0, 0, 0), Mn — 1(b) (0.5, 0.5, 0.5) and O — 3(c) (0.5, 0.5, 0). In the tetragonal phase (space group $I4/mcm$) atomic positions are: Pr/Sr — 4(b) (0, 0.5, 0.25), Mn — 4(c) (0, 0, 0), O1 — 4(a) (0, 0, 0.25), O2 — 8(h) ($x, 1/2 + x, 0$). Values of Mn magnetic moments for C-type tetragonal AFM state of $\text{Pr}_{0.15}\text{Sr}_{0.85}\text{MnO}_3$ obtained at $T = 16$ K are listed

P , GPa	0		2.2		4.0	
T , K	300	16	300	16	300	16
Sp. gr.	$Pm\bar{3}m$	$I4/mcm$	$I4/mcm$	$I4/mcm$	$I4/mcm$	$I4/mcm$
a , Å	3.822(1)	5.359(1)	5.406(1)	5.323(1)	5.391(1)	5.294(1)
c , Å	3.822(1)	7.759(2)	7.568(2)	7.711(2)	7.553(2)	7.685(2)
O2:						
x	—	0.268(3)	0.237(1)	0.267(1)	0.239(1)	0.267(1)
y	—	0.768(3)	0.737(1)	0.767(1)	0.739(1)	0.767(1)
Mn-O1	1.911(1)	1.940(1)	1.892(1)	1.928(1)	1.888(1)	1.921(1)
Mn-O2	—	1.899(1)	1.914(1)	1.887(1)	1.908(1)	1.876(1)
$\angle\text{Mn-O2-Mn}$	—	171 (1)	173.9(6)	172.0(4)	175.1(6)	172.4(4)
μ_{AFM} , μ_B	—	3.0(1)	—	3.2(1)	—	2.8(1)
R_p , %	6.93	8.51	9.72	11.51	10.07	11.75
R_{wp} , %	5.83	7.70	7.84	10.12	9.00	12.33

lected pressures and temperatures and ordered Mn magnetic moments values are presented in Table. At $P = 0$ they agree well with previous investigations [20].

In the tetragonal phase of $\text{Pr}_{0.15}\text{Sr}_{0.85}\text{MnO}_3$ at high pressures and ambient temperature the MnO_6 octahedra are nearly isotropic with about the same Mn-O1 and Mn-O2 bond lengths. The corresponding tetragonal distortion parameter is close to unity, $t = l_{\text{Mn-O1}}/l_{\text{Mn-O2}} \approx 0.989$ at $P = 2.2$ GPa. The onset of the antiferromagnetic long-range order is followed by noticeable elongation of MnO_6 octahedra, the t value increases up to 1.022 at $P = 2.2$ GPa and $T = 16$ K. Such structural distortion is a result of the $d(3z^2 - r^2)$ e_g orbital polarization, characteristic for the C-type AFM ground state [20]. With an increase of pressure at $T = 16$ K (Fig. 6, *a*) the Mn-O2 bond lengths lying in the (*ab*) plane decrease more rapidly in comparison with Mn-O1 bond lengths oriented along the *c*-axis.

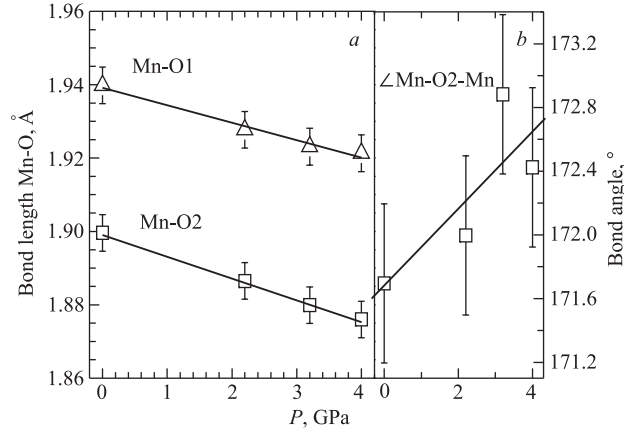


Fig. 6. *a*) Pressure dependences of Mn-O bond lengths in $I4/mcm$ tetragonal phases of $\text{Pr}_{0.15}\text{Sr}_{0.85}\text{MnO}_3$ as functions of pressure at $T = 16$ K. Solid lines represent linear fits to the experimental data. *b*) Pressure dependences of Mn-O2-Mn bond angles in the $I4/mcm$ tetragonal phases of $\text{Pr}_{0.15}\text{Sr}_{0.85}\text{MnO}_3$ at $T = 16$ K

The calculated linear compressibility $k_{\text{Mn-O}i} = (1/(l_{\text{Mn-O}i})_{P=0})(dl_{\text{Mn-O}i}/dP)_T$ ($i = 1, 2$) values for the Mn-O1 bond length, $k_{\text{Mn-O1}} = 0.0025 \text{ GPa}^{-1}$ and $k_{\text{Mn-O2}} = 0.0031 \text{ GPa}^{-1}$ for $\text{Pr}_{0.15}\text{Sr}_{0.85}\text{MnO}_3$ at $T = 16$ K, respectively. Upon compression the Mn-O2-Mn bond angle lying in the (*ab*) plane of the tetragonal structure of $\text{Pr}_{0.15}\text{Sr}_{0.85}\text{MnO}_3$ increases slightly at $T = 16$ K (Fig. 6, *b*). The value of the Mn-O1-Mn bond angle oriented along the *c*-axis is equal to 180° .

The strontium concentration value $x = 0.85$ is located very close to one $x = 0.9$ corresponding to a phase boundary between C-type and G-type AFM states in $\text{Pr}_{1-x}\text{Sr}_x\text{MnO}_3$ [6, 7]. Due to stronger dependence of superexchange AFM interactions with respect to double exchange FM ones on average Mn-O distance, one would expect an occurrence of C-type–G-type AFM transition upon compression according to the predicted theoretical phase diagram [21]. The stability of the C-type AFM state in $\text{Pr}_{0.15}\text{Sr}_{0.85}\text{MnO}_3$ demonstrates that FM

double-exchange interactions along the *c*-axis still remain dominant over AFM superexchange ones over the studied pressure range up to 4 GPa.

CONCLUSIONS

The results of our study show that $\text{Pr}_{0.15}\text{Sr}_{0.85}\text{MnO}_3$ undergoes a structural phase transition from cubic to tetragonal modification upon compression with large and positive pressure coefficient of the transition temperature. The C-type AFM ground state remains stable in the investigated pressure range up to 4 GPa. The pressure coefficient of Neel temperature is also positive but much smaller in comparison with that for the structural transition temperature. Subsequently, while at ambient pressure the onset of the antiferromagnetic long-range order is accompanied by a structural cubic–tetragonal phase transformation, at high pressure structural and magnetic phase transitions become decoupled.

Acknowledgements. The work was supported by the RFBR grant No. 10-02-93163-Mong-a and grant MD-696.2010.2.

REFERENCES

1. Dagotto E., Hotta T., Moreo A. // Phys. Rep. 2001. V. 344. P. 1.
2. Zener C. // Phys. Rev. 1951. V. 82. P. 403.
3. Anderson P. W., Hasegawa H. // Phys. Rev. 1955. V. 100. P. 675.
4. De Gennes P. -G. // Phys. Rev. 1960. V. 118. P. 141.
5. Maezono R., Ishihara I., Nagaosa N. // Phys. Rev. B. 1998. V. 58. P. 11583.
6. Chmaissem O. et al. // Phys. Rev. B. 2003. V. 67. P. 094431.
7. Pollert E. et al. // J. Magn. Magn. Matter. 2002. V. 246. V. 290.
8. Kajimoto R. et al. // Phys. Rev. B. 1999. V. 60. P. 9506.
9. Kozlenko D. P. et al. // J. Phys.: Condens. Matter. 2004. V. 16. P. 2381.
10. Kozlenko D. P. et al. // Phys. Rev. B. 2007. V. 76. P. 094408.
11. Venkateswara P. G. // Phys. Rev. B. 2001. V. 63. P. 064431.
12. Dubrovinskaia N. A., Dubrovinsky L. S. // Rev. Sci. Instrum. 2003. V. 74. P. 3433.
13. Hammersley A. P. et al. // High Press. Res. 1996. V. 14. P. 235.
14. Aksenov V. L. et al. // Physica B. 1999. V. 265. P. 258.
15. Glazkov V. P., Goncharenko I. N. // Fizika i Tekhnika Vysokikh Davlenij. 1991. V. 1. P. 56 (in Russian).
16. Zlokazov V. B., Chernyshev V. V. // J. Appl. Cryst. 1992. V. 25. P. 447.
17. Rodriguez-Carvajal J. // Physica B. 1993. V. 192. P. 55.
18. Birch F. J. // J. Geophys. Res. 1986. V. 91. P. 4949.
19. Kozlenko D. P. et al. // Phys. Rev. B. 2007. V. 75. P. 104408.
20. Martin C. et al. // J. Magn. Magn. Matter. 1999. V. 205. P. 184.
21. Maitra T., Taraphder A. // Phys. Rev. B. 2003. V. 68. P. 174416.

Received on March 1, 2010.

Редактор *В. В. Булатова*

Подписано в печать 19.04.2010.

Формат 60 × 90/16. Бумага офсетная. Печать офсетная.

Усл. печ. л. 0,75. Уч.-изд. л. 1,03. Тираж 290 экз. Заказ № 56967.

Издательский отдел Объединенного института ядерных исследований
141980, г. Дубна, Московская обл., ул. Жолио-Кюри, 6.

E-mail: publish@jinr.ru

www.jinr.ru/publish/